Rational control of typical surface defects of hybrid perovskite using tetrahexylammonium iodide

Ben Wang[1], Shunwei Yao[1], Wenjing Hu[1], Lin Peng[1]*, Tingting Shi[2], Yanan Wang[1], Jing Chen[1], Xiaolin Liu[1], and Jia Lin[1]*

[1]Department of Physics, Shanghai University of Electric Power, Shanghai 200090, China

[2]Department of Physics, Jinan University, Guangzhou 510632, China

*Corresponding authors: Lin Peng, Email: plpeng@shiep.edu.cn
Jia Lin, Email:jlin@shiep.edu.cn

The convergence checks for slab size and vacuum layer

We examined the convergence of slab size and vacuum layer by calculating the defect formation energy of iodine vacancy (V_I) on the surface of $FAPbI_3$. From the energy point of view (Fig. S1), the size of 3×3 is close to convergence. Considering the size of the system and the limitation of computing resources, we choose the size of 3×3 $FAPbI_3$ slab to carry out the related calculation of defect properties. The thickness of vacuum layer has little influence on the forming energy of neutral defect [Ref. S1]. According to the calculated results (Fig. S2), it can be seen that the formation energy of V_I has reached convergence at 30 Å.

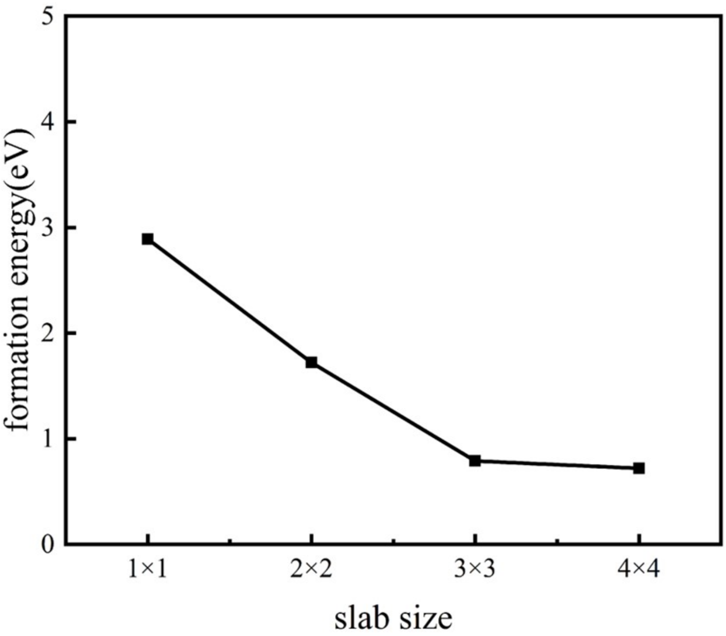

Fig. S1. Convergence of formation energy of V_I with different sizes of slab.

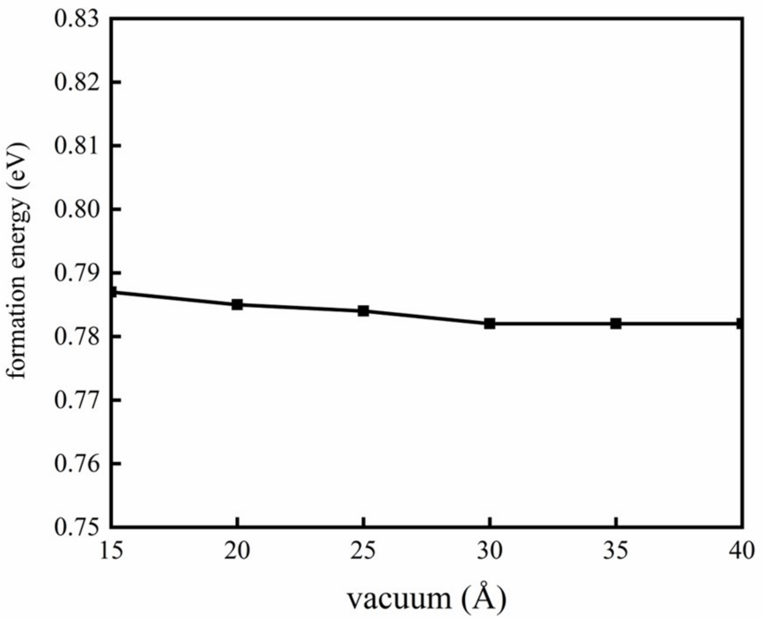

Fig. S2. Convergence of formation energy of $V_I$with different thicknesses of vacuum layer. The slab size is 3×3.

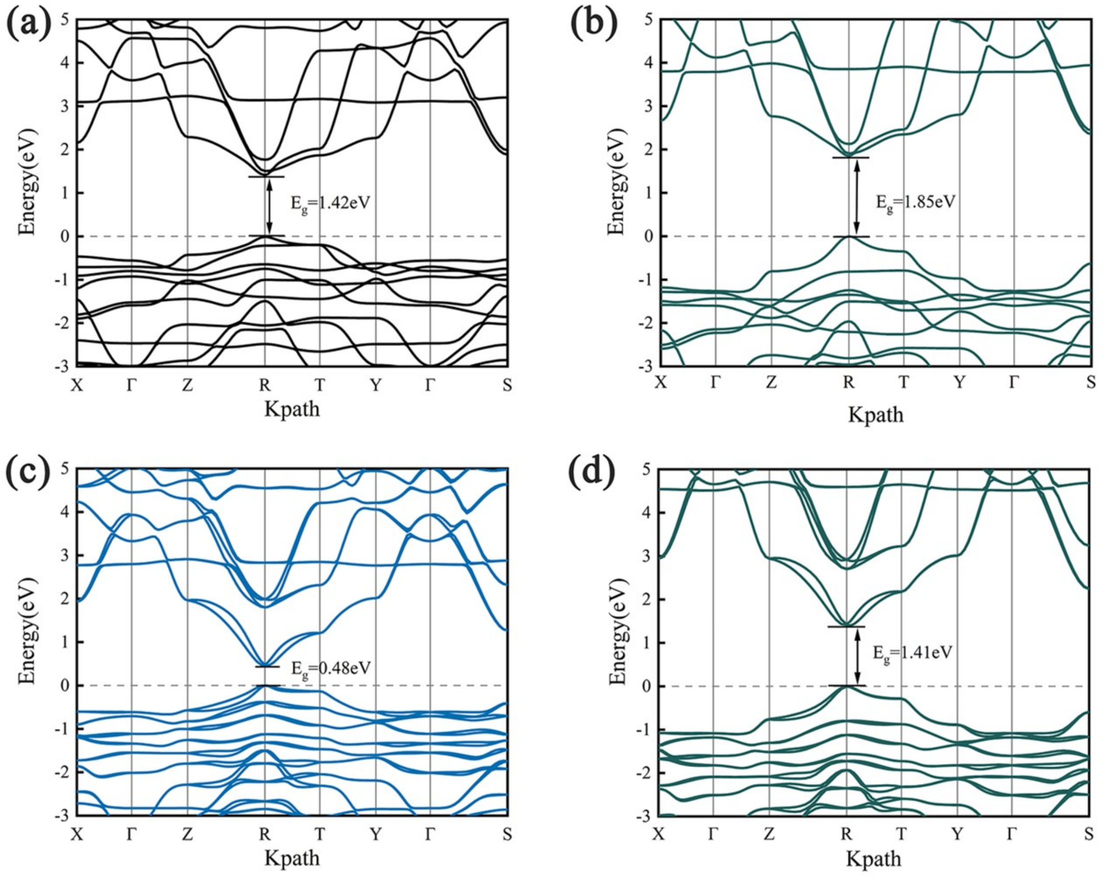

Fig. S3. The band structure of $FAPbI_3$ without defects was calculated using different methods: (a) PBE, (b) HSE (α=0.25), (c) PBE+SOC and (d) HSE+SOC (α=0.41).

Table S1. Calculated band gap (eV) of $FAPbI_3$ using PBE compared with experimental value and reported theoretical value [37,41].

Calculated value	Experimental value	Theoretical value
1.424	1.43	1.418

Table S2. The lattice distortion degree ($amu^{1/2}$Å) of $FAPbI_3$ surface with different defects.

V_I	V_{Pb}	Pb_I	I_{Pb}
43.11	55.75	46.60	77.04

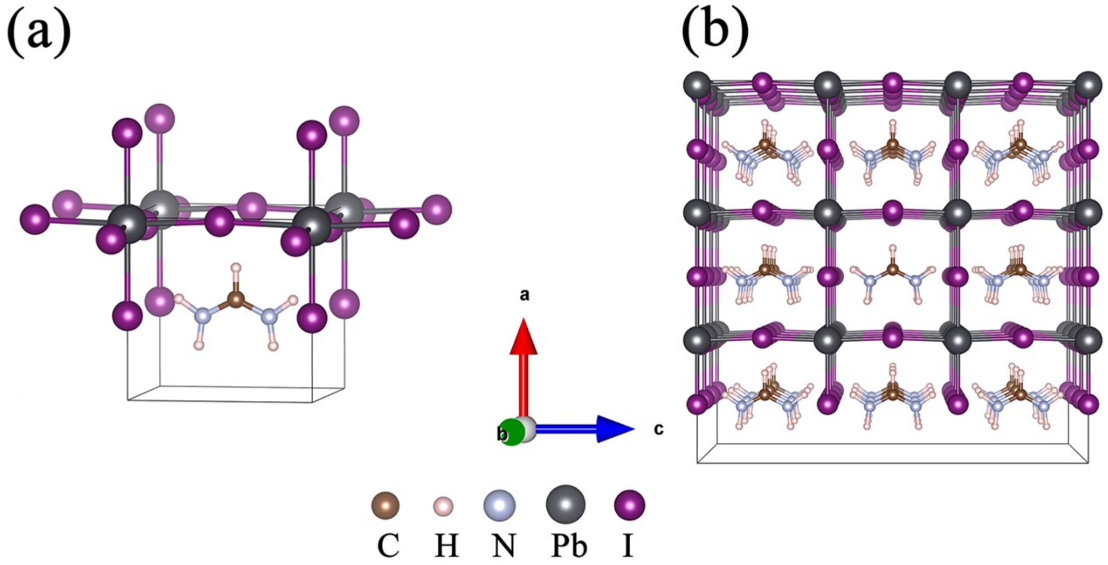

Fig. S4. (a) Original cell of $FAPbI_3$ and (b) the PbI_2-terminated (1 0 0) surface of $FAPbI_3$.

Chemical Potential Calculations

When $FAPbI_3$ is formed as a stable phase the chemical potentials should follow:

$$\mu_{FA} + \mu_{Pb} + 3\mu_I = \Delta H^f(FAPbI_3) = -5.44eV \qquad (S1)$$

where $\Delta H^f(FAPbI_3)$ is the formation energy of $FAPbI_3$.To prevent from the formation of competitive secondary compounds FAI and PbI_2, the following conditions should be satisfied:

$$\mu_{FA} + \mu_I < \Delta H^f(FAI) = -2.83eV \qquad (S2)$$

$$\mu_{Pb} + 2\mu_I < \Delta H^f(PbI_2) = -2.13eV \qquad (S3)$$

Base on the Eqs. (S1)-(S3), the chemical potential region for the equilibrium growth condition of $FAPbI_3$ was calculated, as shown in Fig. S5. Three representative chemical potential points labled as A (I-rich), B (Moderate), and C (Pb-rich). The values of chemical potentials calculated at the PBE level are: A ($\mu_{FA} = -2.83eV, \mu_{Pb} = -2.61eV, \mu_I = 0eV$), B ($\mu_{FA} = -2.18eV, \mu_{Pb} = -1.31eV, \mu_I = -0.65eV$), and C ($\mu_{FA} = -1.53eV, \mu_{Pb} = 0eV, \mu_I = -1.31eV$).

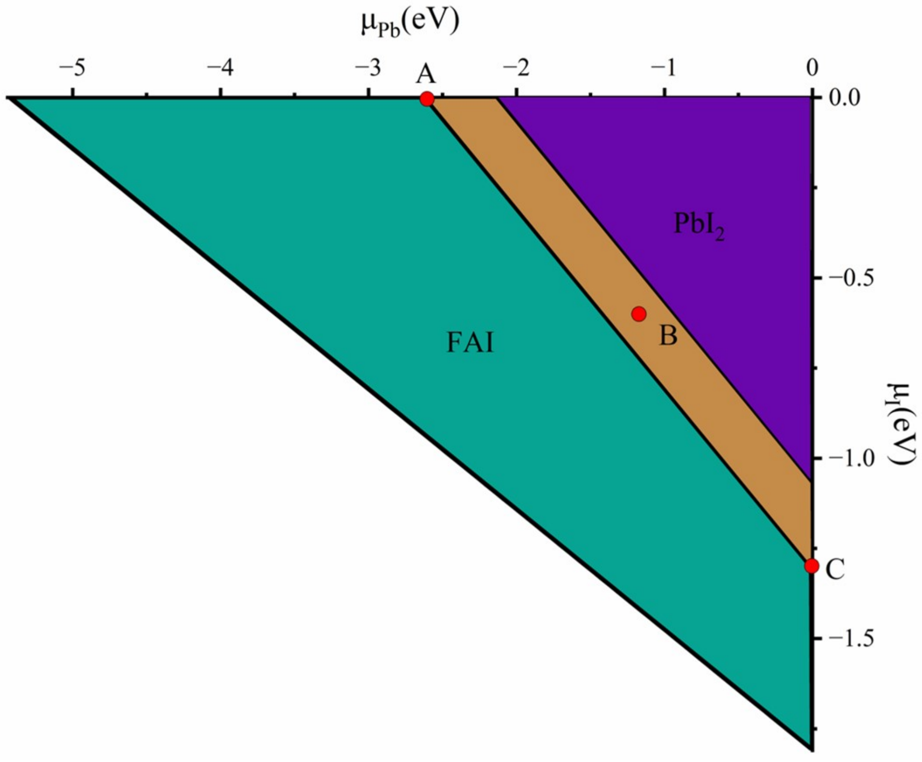

Fig. S5. Phase diagram of chemical potential calculated at the PBE level for the thermal equilibrium growth of $FAPbI_3$. The brownness-shaded area shows the region where $FAPbI_3$ is thermodynamically stable. The points A, B and C mark three representative sets of chemical potentials.

Energy Corrections

Freysoldt-Neugebauer-van de Walle (FNV) type correction scheme is considered for the finite-size corrections. [45]

$$E^{corr}_{q} = E^{latt}_{q} - q\Delta V \qquad (S4)$$

Where E^{latt}_{q} is the lattice correction, and ΔV is the potential alignment of the charged defect relative to the model periodic lattice potential far from the defect.

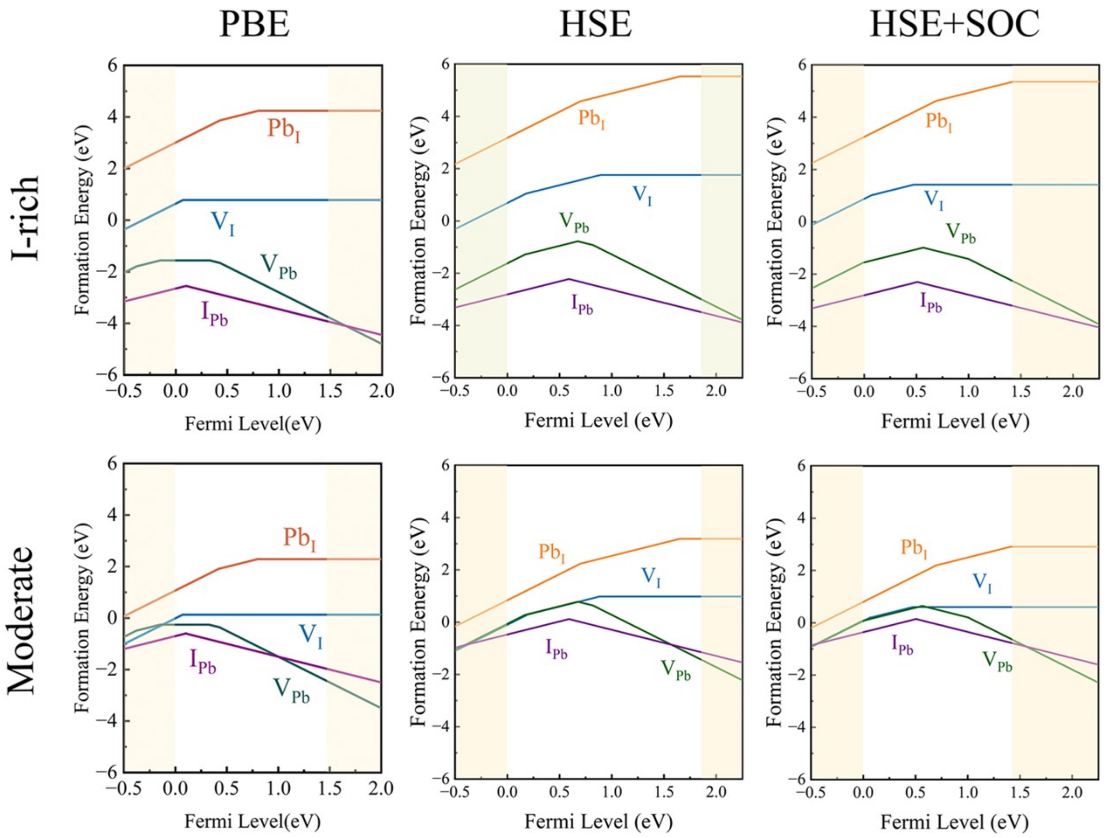

Fig. S6. The formation energies of defects with respect to the Fermi level calculated with different functionals under the I-rich and Moderate growth condition: PBE; HSE (α=0.25); HSE+SOC (α=0.41).

Electron Localization Function (ELF) Calculations

The function of ELF [46,47]:

$$\eta(\vec{r}) = \frac{1}{1 + [D(\vec{r})/D_h(\vec{r})]^2} \qquad (S5)$$

where

$$D(\vec{r}) = \frac{1}{2}\sum_{j=1}^{N} \left|\nabla \emptyset_j(\vec{r})\right|^2 - \frac{1\nabla\rho(\vec{r})^2}{8\ \ \rho(\vec{r})} \qquad (S6)$$

$$D_h(\vec{r}) = \frac{3}{10}(3\pi^2)^{2/3}\rho(\vec{r})^{5/3} \qquad (S7)$$

$$\rho(\vec{r}) = \sum_{j=1}^{N} \left|\emptyset_j(\vec{r})\right|^2 \qquad (S8)$$

Here, N is the number of electrons.

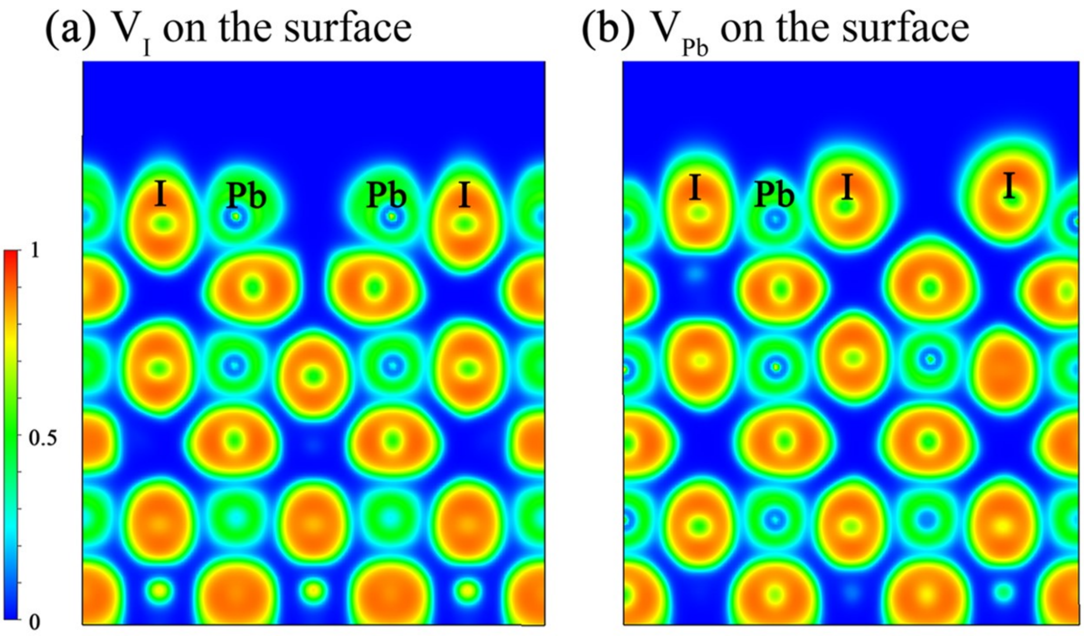

Fig. S7. 2D cross-sectional view of the ELF field for the defects on the $FAPbI_3$ surface: (a) V_I and (b) V_{Pb}. One means complete electron localization, and zero means complete electron delocalization on the left scale plane.

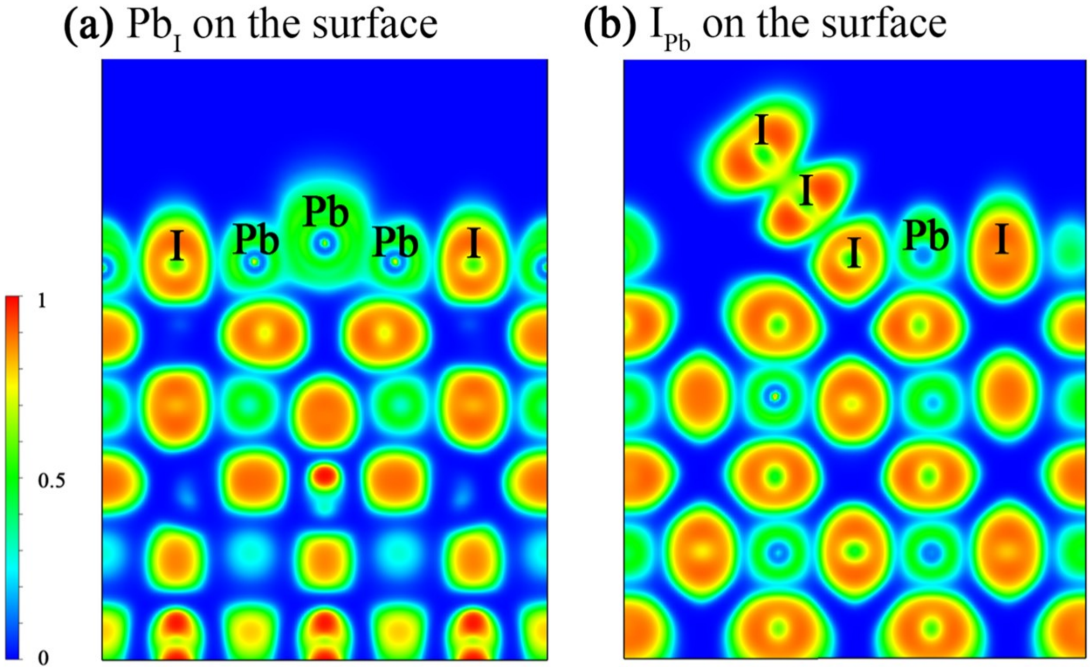

Fig. S8. 2D cross-sectional view of the ELF field for the defects on the FAPbI$_3$ surface: (a) Pb$_I$ and (b) I$_{Pb}$. One means complete electron localization, and zero means complete electron delocalization on the left scale plane.

Table S3. The lengths (Å) of coordination bonds and hydrogen bonds formed by THAI adsorbed on $FAPbI_3$ (1 0 0) surface with different defects.

Types of defects	$d_{Pb\text{-}I}$ (Å)	Atomic serial number	$d_{I\text{-}H}$ (Å)	Atomic serial number
V_I	3.21	Pb23-I81	3.11	I67-H139
	3.29	Pb24-I81	-	-
V_{Pb}	2.95	Pb23-I82	2.99	I37-H139
Pb_I	3.12	Pb24-I81	3.11	I69-H150
	3.25	Pb23-I81	2.78	I67-H167
I_{Pb}	2.97	Pb25-I83	2.96	I67-H150
	-	-	3.04	I58-H138

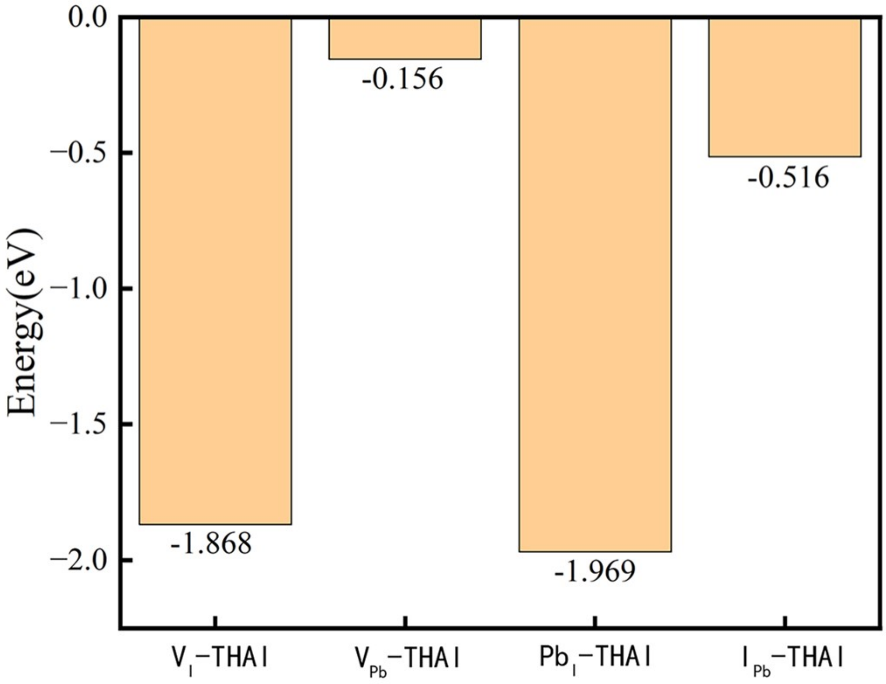

Fig. S9. Adsorption energies (eV) for THAI adsorbed on $FAPbI_3$ surface containing defects.

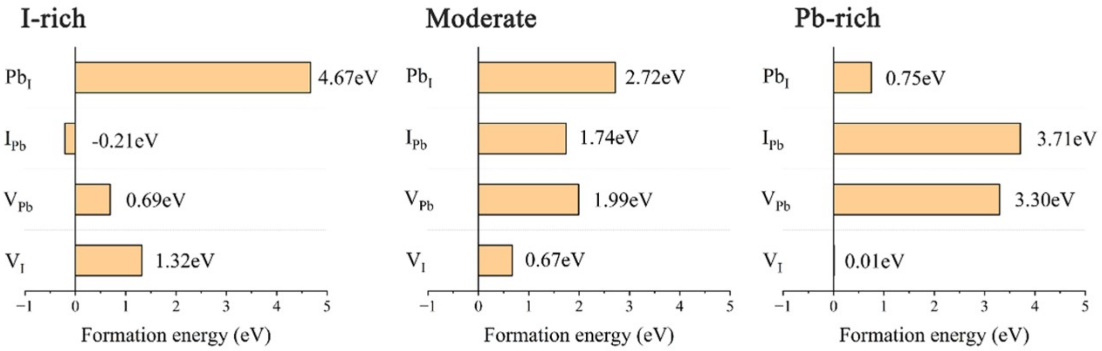

Fig. S10. Formation energies of neutral defects under the different growth conditions for the system of $FAPbI_3$ with THAI.

For Pb_I, the calculated results of charge transition levels and formation energies are shown in Table 3 and Fig. S11. The formation energy of Pb_I increased under different growth environments after THA+ and I- were added separately, indicating that THA+ and I- both had inhibitory effects on Pb_I. In addition, after adding THA+, the (-1/-2) level appears in a shallow position (0.3eV); after adding I-, the (+1/0) level is 0.15 eV. Therefore, both THA+ or I- have a passivation effect on surface defects. The THA+ could interact with halogen ions on the surface of perovskite by forming hydrogen bonds, and the I- could interact with lead ions on the surface of perovskite by forming coordination bonds. When THAI is used as a passivant, it can interact with different defects on the surface of the perovskite and enhance the stability of the perovskite structure.

Table S4. Formation energies under the different growth conditions and thermodynamic charge transition levels of Pb_I for the system of $FAPbI_3$ with THAI, THA+, and I-.

		with THAI	with THA+	with I-
DFEs (eV)	I-rich	4.67	5.11	5.29
	Moderate	2.72	3.16	3.34
	Pb-rich	0.75	1.19	1.37
Transition level (eV)	(+1/0)	1.03	-	0.15
	(-1/-2)	-	0.3	-

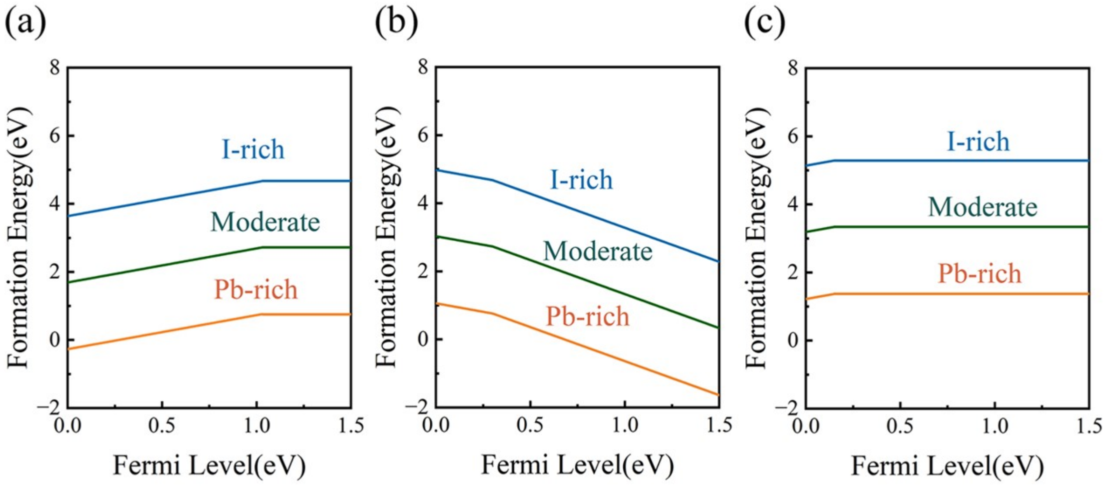

Fig. S11. The formation energies of Pb_I with respect to the Fermi level for the systems of $FAPbI_3$ with THAI (a), $FAPbI_3$ with THA+ (b) and $FAPbI_3$ with I- (c).

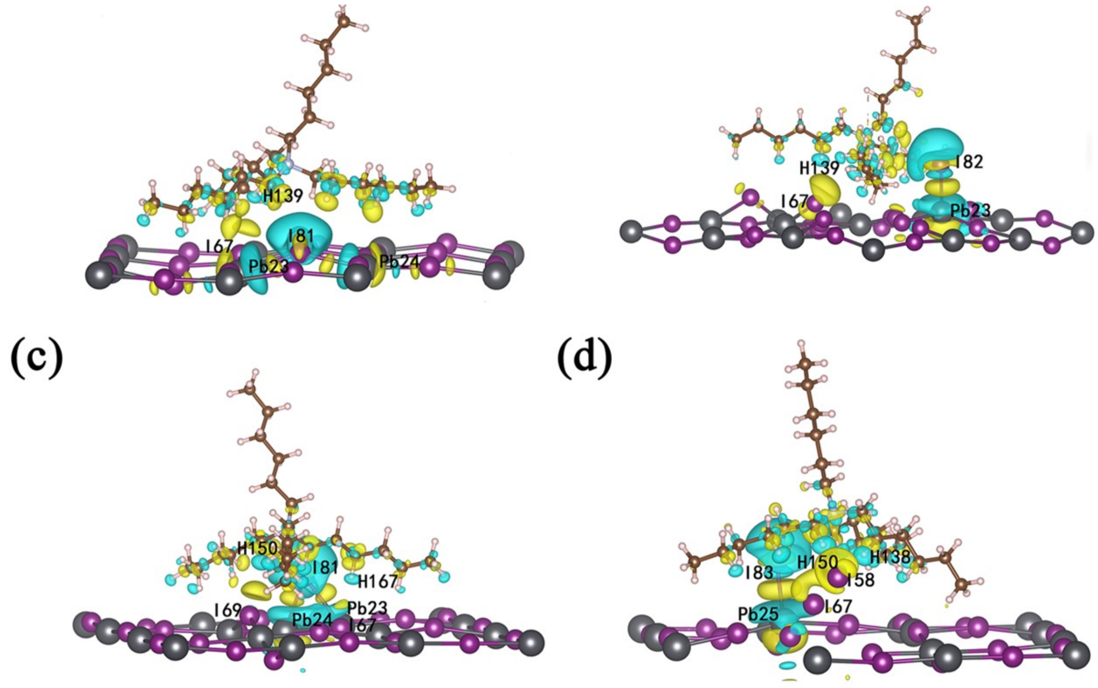

Fig. S12. CDD for the adsorption systems of THAI/FAPbI$_3$: (a) V_I, (b) V_{Pb}, (c) Pb_I and (d) I_{Pb}. Charge accumulation and depletion are indicated by the colors yellow and cyan.

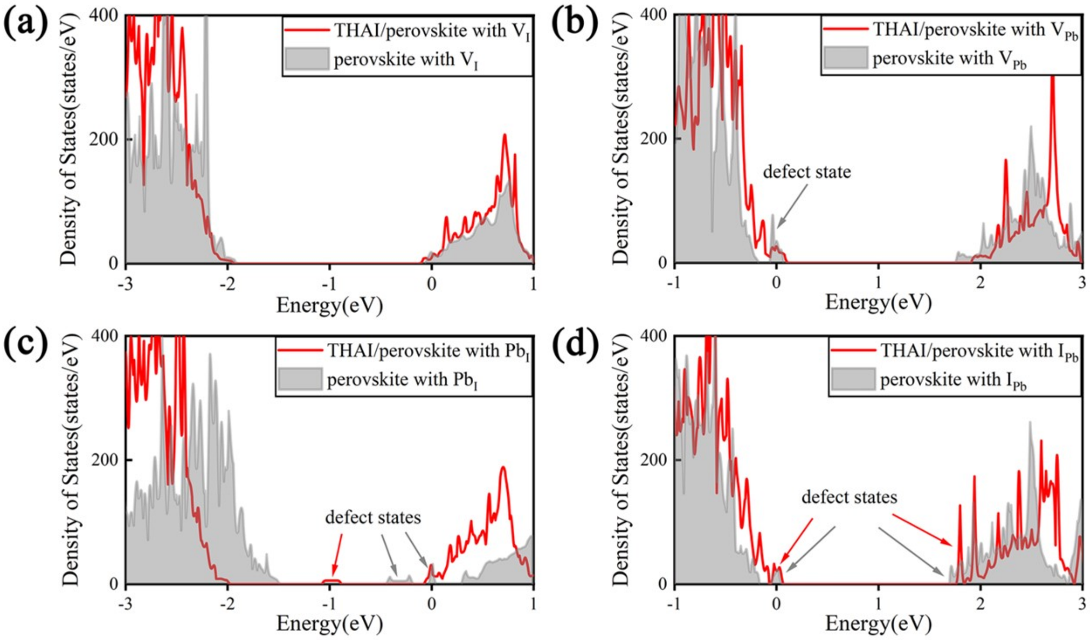

Fig. S13. Total DOS of $FAPbI_3$ containing surface defects with and without THAI adsorption: (a) V_I, (b) V_{Pb}, (c) Pb_I and (d) I_{Pb}.

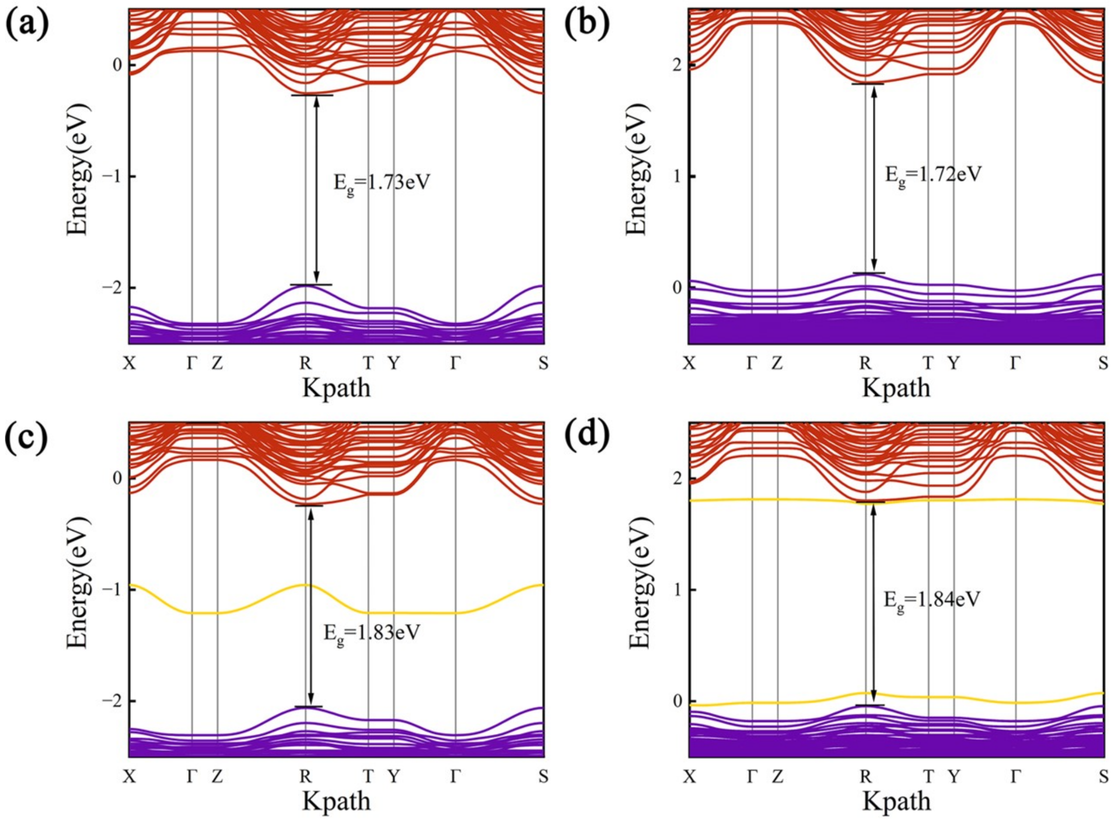

Fig. S14. Band structures of $FAPbI_3$ containing surface defects with THAI adsorption: (a) V_I, (b) V_{Pb}, (c) Pb_I and (d) I_{Pb}. The Fermi level is set to 0. The yellow solid lines denote defect levels.

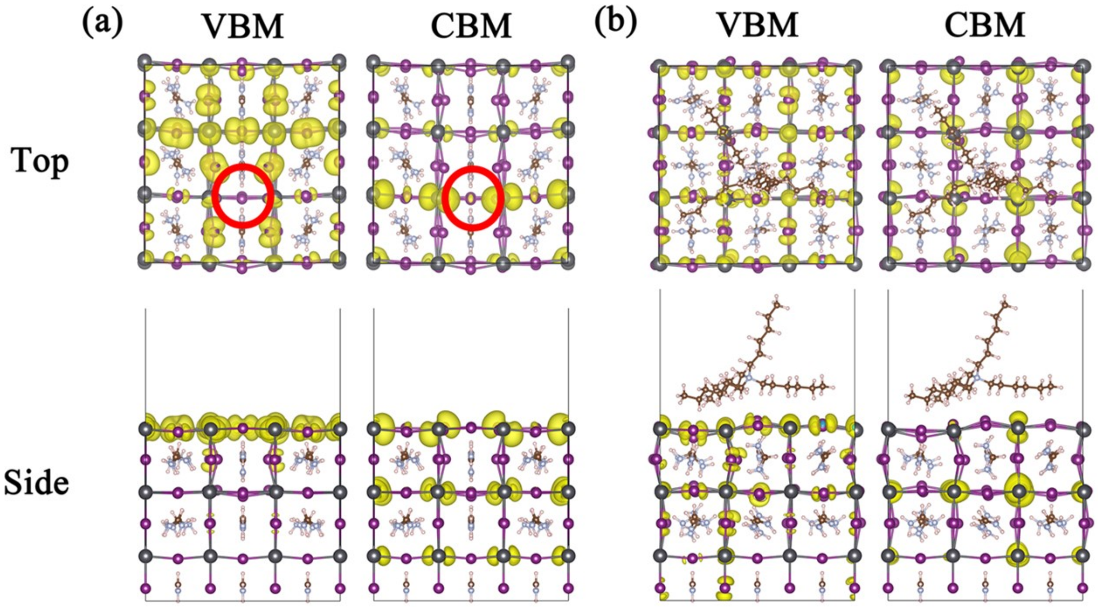

Fig. S15. Band decomposed charge densities distribution of V_I on the $FAPbI_3$ surface without (a) or with (b) THAI adsorption for VBM and CBM. The locations of defects are highlighted by solid red circles.

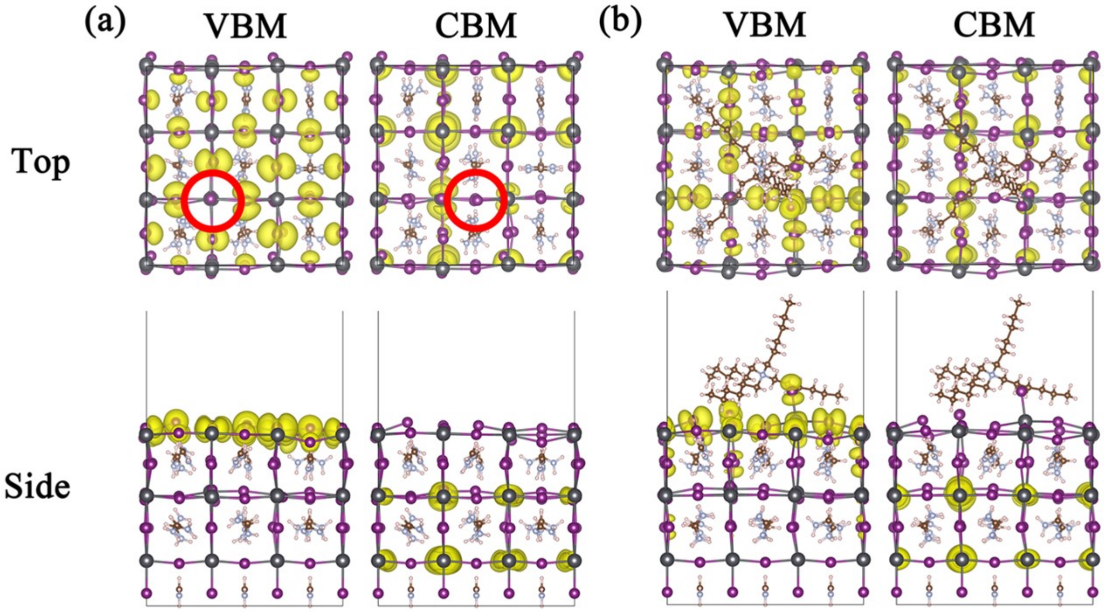

Fig. S16. Band decomposed charge densities distribution of V_{Pb} on the $FAPbI_3$ surface without (a) or with (b) THAI adsorption for VBM and CBM. The locations of defects are highlighted by solid red circles.

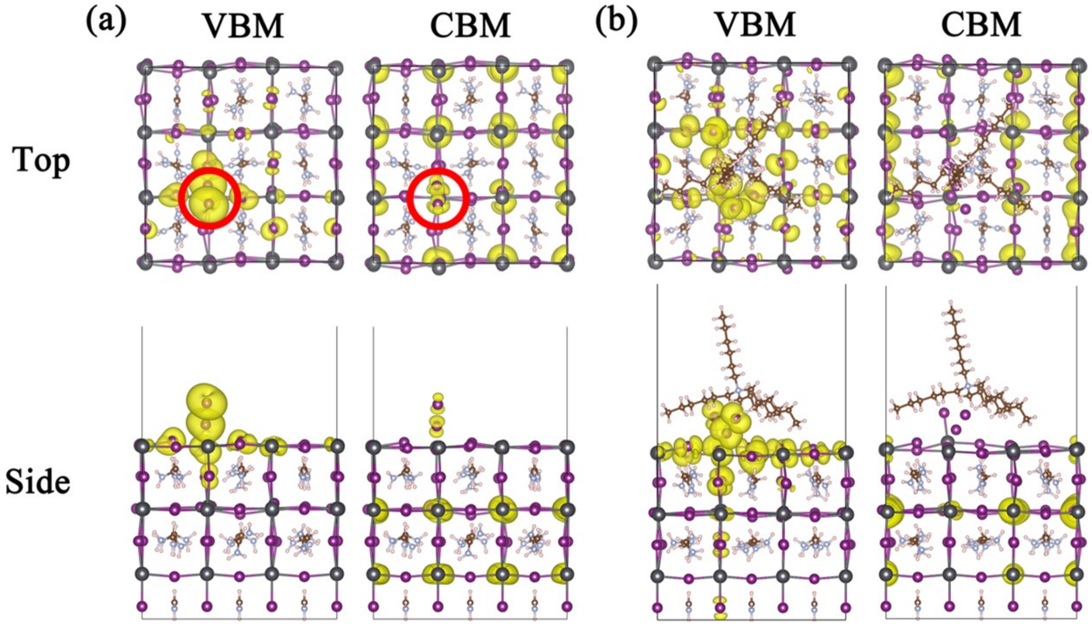

Fig. S17. Band decomposed charge densities distribution of I_{Pb} on the $FAPbI_3$ surface without (a) or with (b) THAI adsorption for VBM and CBM. The locations of defects are highlighted by solid red circles.

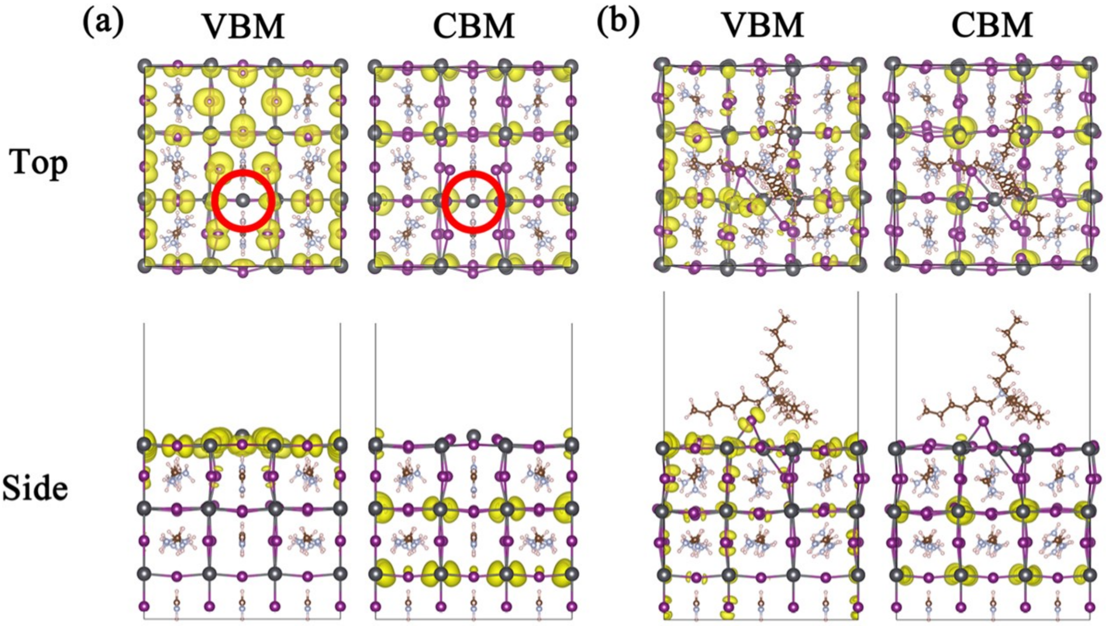

Fig. S18. Band decomposed charge densities distribution of Pb_I on the $FAPbI_3$ surface without (a) or with (b) THAI adsorption for VBM and CBM. The locations of defects are highlighted by solid red circles.

Shorter alkyl chain lengths

We used tetrabutylammonium iodide (TBAI) as a passivating agent to interact with V_{Pb}, which has four C atoms on each alkyl chain. Through structural optimization and ELF calculation results [Fig. S18(a, b)], we can observe the formation of I trimers. The adjacent I atoms form bonds with the I atom in TBAI, forming a trimer structure of I with bond lengths of 2.91 and 2.96 Å, respectively. In order to further illustrate the intense reaction between TBAI and the defective surface of $FAPbI_3$, we analyzed the charge density difference (CDD) of this adsorption system. The CDD diagram [Fig. S18(c)] reveals that charge accumulation regions are present between the I atom in TBAI and the I atom in perovskite, indicating the strong bonding of the I and I atoms. In the meantime, the existence of charge accumulation regions between I atom in perovskite and H atom in TBAI signifies the formation of I…H hydrogen bonds.

Subsequently, through the calculation of electron density of states [Fig. S18(d)], it is found that after the adsorption of TBAI, the defect state near the Fermi level is not eliminated, and the local electron state also appears near the CBM. This may be due to the formation of I trimer structure after TBAI adsorption. We believe that TBAI with short alkyl chain length cannot passivate V_{Pb}. THAI could better passivate V_{Pb} and completely eliminate the local electronic states in the band gap. Therefore, in this work, we mainly discussed THAI as a passivating agent to passivate surface defects.

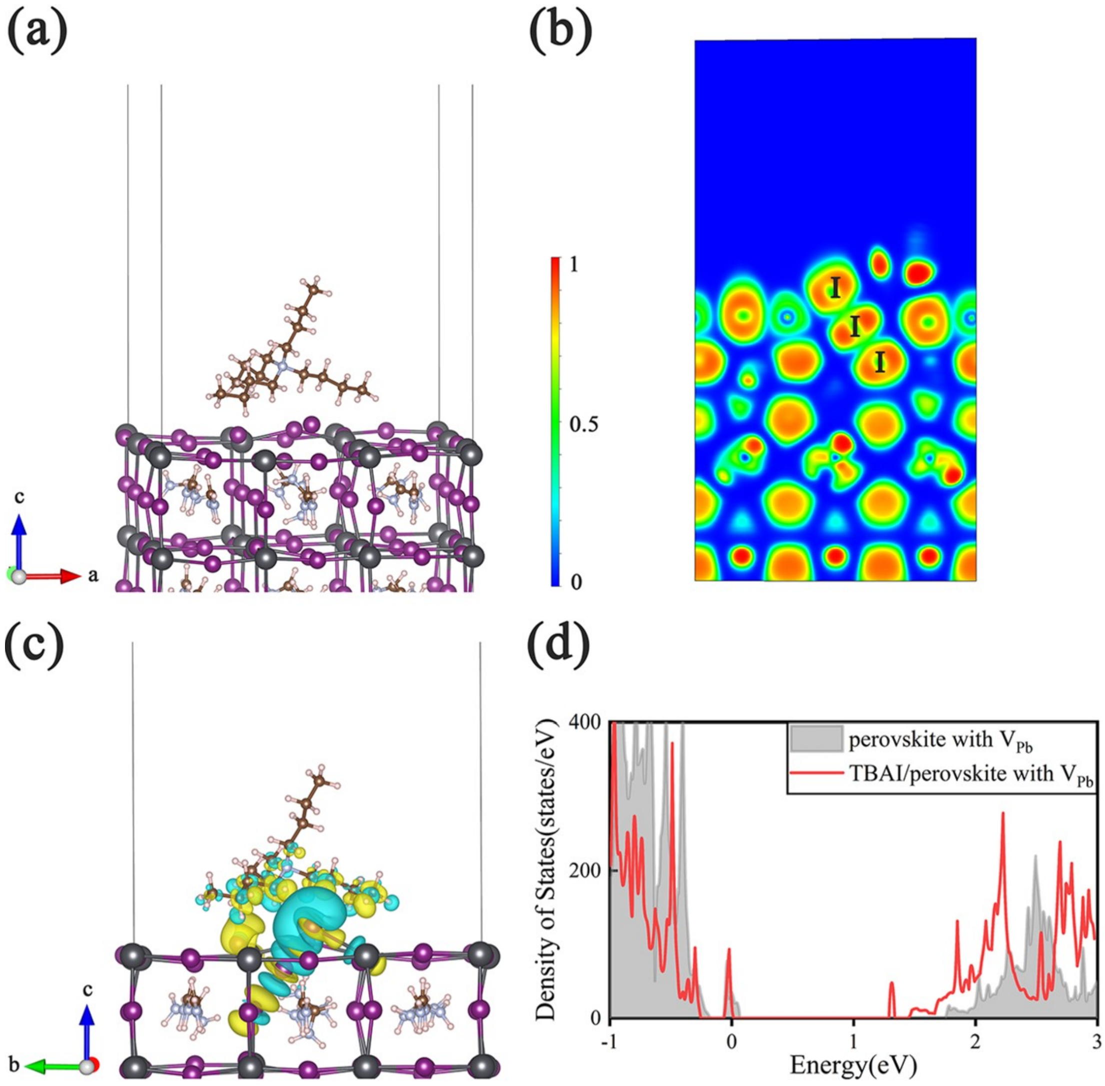

Fig. S18. (a) Optimized geometric model of V_{Pb}/TBAI. (b) 2D cross-sectional view of the ELF field for the system of V_{Pb}/TBAI. One means complete electron localization, and zero means complete electron delocalization on the left scale plane. (c) CDD for the adsorption systems of V_{Pb}/TBAI. Charge accumulation and depletion are indicated by the colors yellow and cyan. (d) Total DOS of $FAPbI_3$ containing V_{Pb} with and without TBAI adsorption.

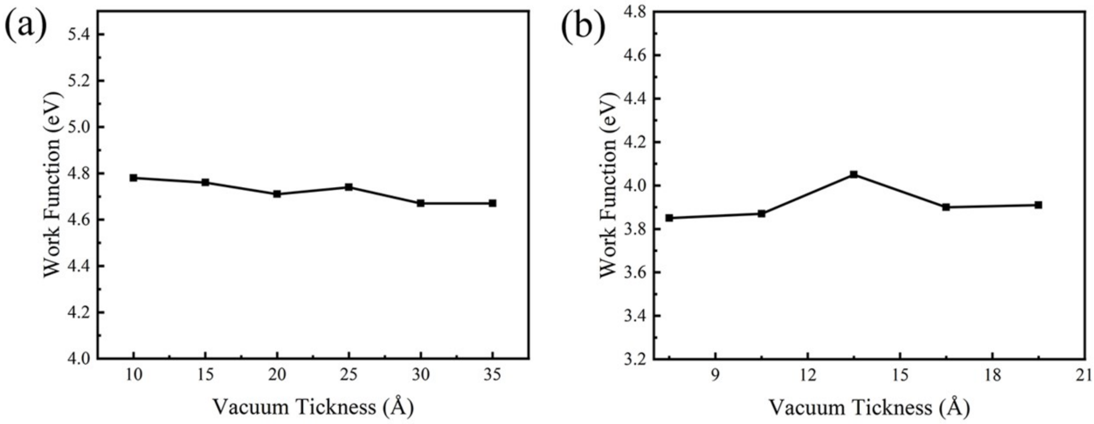

Fig. S19. Calculated work functions of (a) $FAPbI_3$ and (b) the adsorption systems of THAI/$FAPbI_3$, as a function of the vacuum thickness in the repeated-slab unit cell.

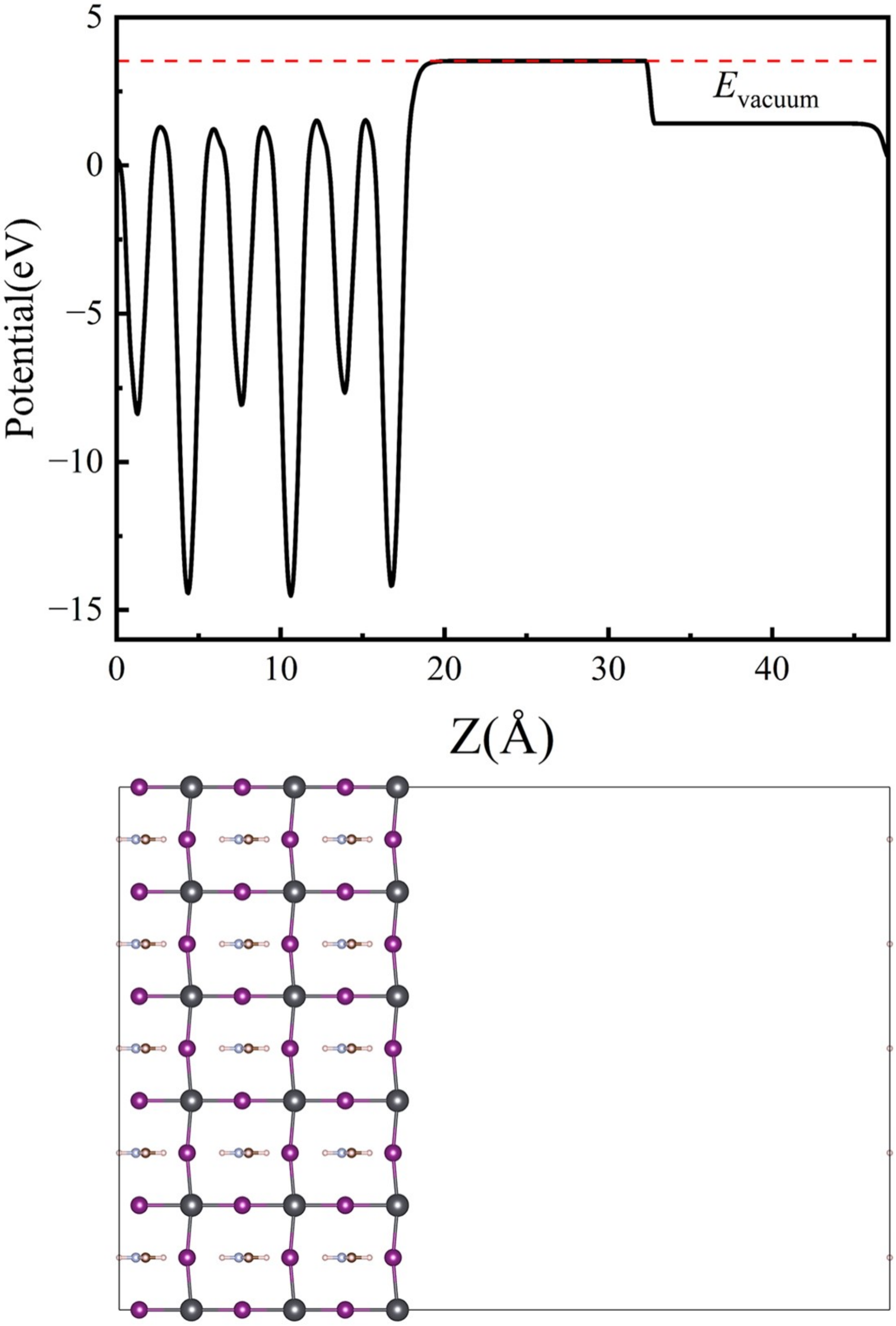

Fig. S20. Electrostatic potential of $FAPbI_3$ along the *z* direction.

REFERENCES

[S1] C. Freysoldt and J. Neugebauer, First-principles calculations for charged defects at surfaces, interfaces, and two-dimensional materials in the presence of electric fields, Phys. Rev. B **97**, 205425 (2018).